



# OPEN Metasurface-integrated Al<sub>2</sub>O<sub>3</sub> ceramic dielectric resonator for enhanced gain and polarization performance in mm-wave MIMO systems

Sateesh Kumar Yadav<sup>1</sup>, Ajay Kumar Dwivedi<sup>2</sup>, Deepak Sigroha<sup>3</sup>, Shivesh Tripathi<sup>4</sup>, Anand Sharma<sup>1</sup> & Stuti Pandey<sup>5</sup>✉

This paper outlines the design and characterization of a dual-port dielectric resonator antenna made from alumina (Al<sub>2</sub>O<sub>3</sub>) and coupled with a metasurface superstrate for millimeter-wave applications. Alumina ceramic with high permittivity ( $\epsilon_r = 9.9$ ,  $\tan\delta = 0.0019$ ) was employed to excite the lower-order HEM<sub>11 $\delta$</sub>  mode through aperture coupling to enable efficient radiation between 27.65 and 28.75 GHz. A dual-stub C-shaped slot was carefully engineered on the substrate to generate orthogonal modes, thereby realizing circular polarization throughout the bandwidth of 27.8–28.45 GHz. To access better radiation properties, a double-negative (DNG) metasurface lens made on an RT Duroid substrate was coupled with a resultant increase in realized gain to about 11 dBi, with preservation of impedance and polarization properties. Experimental characterization confirmed steady broadside radiation patterns with low mutual coupling ( $< -25$  dB), together with exemplary diversity parameters (ECC  $< 0.02$ , DG  $\approx 10$  dB). The integration of both dielectric ceramic and metasurface building materials demonstrates a synergistic building–structure approach to realizing high-gain, circularly polarized, volume-reduced radiators with millimeter-wave applications. These outcomes highlight engineered dielectric–metasurface architectures as a prospective pathway for licensed 5G FR2 frequency band.

**Keywords** Dielectric antenna, Circular polarization, High gain, Mm-wave

In the present era of wireless communication, the working spectrum is moving to higher frequency bands, i.e., mm-wave, to get a high data rate with the assistance of getting a larger bandwidth. There are lots of challenges that appeared during the shift from the lower frequency band to the higher one, such as large path loss and small antenna gain<sup>1</sup>. One of the remedies for these challenges are multi-port antenna design, which improves the signal-to-interference ratio without further increment in signal power<sup>2</sup>. The problem associated with aerial gain in mm-wave can be reduced with the help of ceramic-built aerials due to the absence of metallic parts<sup>3,4</sup>. Circular polarization is an important feature in mm-wave antennas because it originates the capability to receive the signal, even if there is a mismatch in transmitter and receiver orientation<sup>5</sup>.

A few articles about mm-wave multi-port dielectric antennas can be found in the literature. Zhang and colleagues developed a dielectric resonator aerial with two ports that operates in the 27.25–28.59 GHz. A copper strip over the dielectric reduced the coupling level to  $-12$  dB<sup>6</sup>. To increase the isolation level between two ports, Pan et al. structured a unique technique that uses vias. In between 25.0 and 27.0 GHz range, this aerial design works with a separation of over 40 dB<sup>7</sup>. Using the concept of a conducting strip over a dielectric, N S Murthy increased the isolation among the four ports. Between 26.6 and 29.57 GHz, this aerial works with an isolation of around 17 dB<sup>8</sup>. A two-port ceramic antenna was built by Hasan et al. with an incorporated isolator between the

<sup>1</sup>Department of Electronics and Communication Engineering, Motilal Nehru National Institute of Technology Allahabad, Prayagraj, UP, India. <sup>2</sup>Department of Electronics and Communication Engineering, Cambridge Institute of Technology, K. R. Puram, Bangalore 560036, Karnataka, India. <sup>3</sup>Department of Electronics Engineering, Rajkiya Engineering College, Sonbhadra, UP, India. <sup>4</sup>Department of Electronics and Communication Engineering, G L Bajaj Institute of Technology and Management, Greater Noida, UP, India. <sup>5</sup>Department of Artificial Intelligence and Machine Learning, Manipal University Jaipur, Jaipur, Rajasthan, India. ✉email: stuti.pandey@jaipur.manipal.edu

ports to increase separation. Between 58.8 and 63.6 GHz, it operates with a separation of 40 dB<sup>9</sup>. Alanazi and colleagues constructed an aperture-connected square dielectric at mm-wave. The antenna is positioned on the reverse edge of the substrate, which offers separation of around 27 dB for 27.9–28.8 GHz spectrum<sup>10</sup>. Mm-wave two-port ceramic was planned by Kumar et al. It takes advantage of a plus-shaped slot to produce circular waves inside the operational spectrum, which is 25.5–27.79 GHz<sup>11</sup>. The working spectrum of the 2-port dielectric-built filtering radiator that Sharma et al. developed is 27.8–28.5. By placing anti-parallel ports, the isolation is raised to above 30 dB<sup>12</sup>. Nipun et al. recently designed two different multi-port radiating designs loaded with single negative MS. This type of MS reduces the coupling value among the antenna ports<sup>13,14</sup>. Ibrahim et al. designed two different multi-port circularly polarised Dielectric antennas. In the first one, CP waves are created by deformation of ceramic blocks, while the second one supports circular E-field using stair-shaped dielectric<sup>15,16</sup>.

This research article develops the ceramic-built 2-port aerial in the mm-wave spectrum. Two features are added with the designed aerial: (i) a feeding structure produces the CP waves within the working spectrum; and (ii) a metasurface lens is used to improve the antenna gain (12 dBi) in the mm-wave regime. To better understand the concept, this paper is separated in sectors: (a) aerial layout model; (b) aerial examination; (c) measured results; and (d) inference.

### Aerial design and its dimensions

Figure 1 exhibits the structural arrangement of the planned aerial. This radiator is designed on the RT Duroid base ( $\epsilon_r = 2.1$  and  $\tan\delta = 0.01$ ), having a depth 0.255 mm. On the top side of the dielectric base, a C-formed slot with dual stubs has been etched.  $\text{Al}_2\text{O}_3$  ceramic ( $\epsilon_r = 9.9$  and  $\tan\delta = 0.0019$ ), which is set above the aperture, is stimulated by it. Microrstrip is intended to feed an etched aperture on the bottom of the substrate. The RT Duroid base is also used to create a Metasurface lens. The description of Fig. 1 mentions the optimal dimensions of diverse parameters of the planned aerial.

### Antenna examination

This segment performs the detailed analysis of the planned aerial via HFSS software. Investigation begins with a 1-port aerial. Figure 2 presents the alteration of  $|S_{11}|$  with various cases taken in a single port aerial: (a) aperture without ceramic; (b) ring slot coupled ceramic; (c) C-shaped slot coupled ceramic; (d) C-shaped slot with dual stubs coupled dielectric. Several significant findings from Fig. 2 are: (i) the whole operational spectrum is due to alumina dielectric; (ii) in the presence of ceramic, the resonant peak appears at 28.0 GHz; and (c) C-shaped slot with dual stubs improves the working bandwidth because of the formation of orthogonal mode. The E-field traces within the dielectric at 28.0 GHz are seen in Fig. 3. It shows that the  $\text{HEM}_{116}$  mode is created within

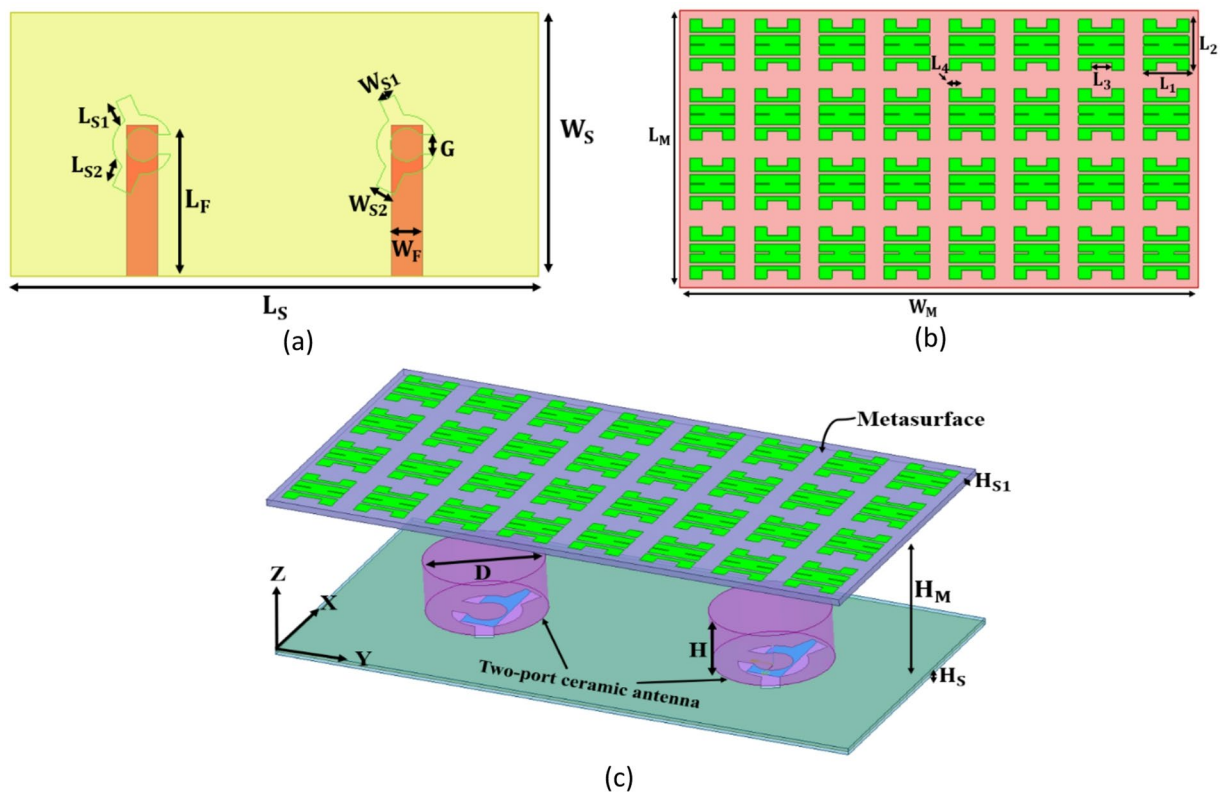


**Fig. 1.** Arrangement of Planned 2-port Ceramic Radiator (a) Feed Design (b) Metasurface Design (c) 3D View;  $L_S = 40.0$ ;  $W_S = 20.0$ ;  $L_{S1} = 1.0$ ;  $L_{S2} = 1.25$ ;  $W_{S1} = 1.0$ ;  $W_{S2} = 1.25$ ;  $H_S = 0.254$ ;  $H_{S1} = 0.254$ ;  $H_M = 5.0$ ;  $D = 6.0$ ;  $H = 3.0$ ;  $W_M = 40.0$ ;  $L_M = 20.0$ ;  $L_F = 10.0$ ;  $W_F = 2.0$ ;  $L_1 = 3.0$ ;  $L_2 = 4.0$ ;  $L_3 = 1.0$ ;  $L_4 = 0.5$ ;  $G = 1.0$  (in mm).

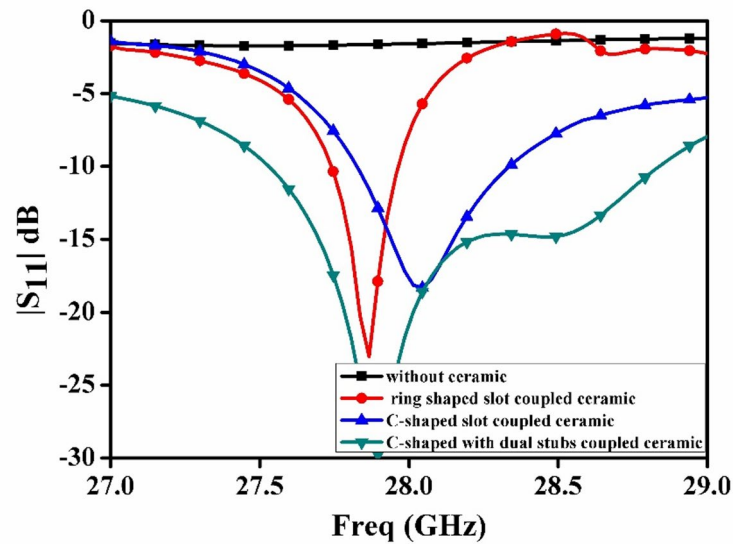


Fig. 2. Change in  $|S_{11}|$  with diverse modifications in the shape of the slot.

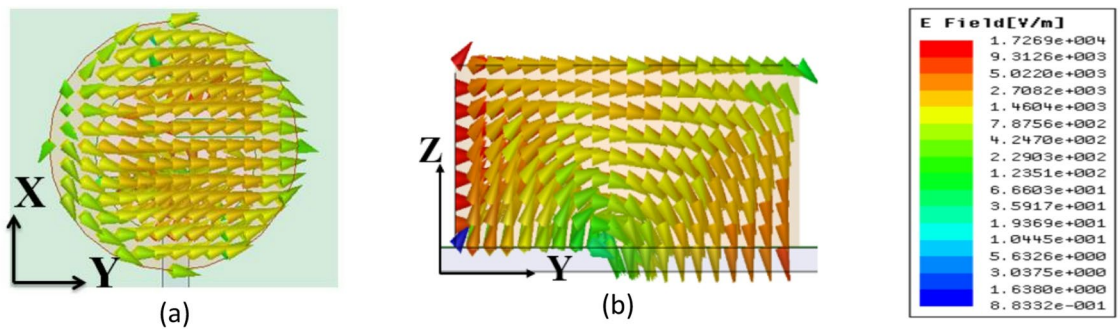


Fig. 3. E-field lines on Alumina dielectric at 28.0 GHz (a) Upper Sight (b) Lateral Sight.

the dielectric. A slot acts magnetic dipole; therefore, it produces a fundamental hybrid mode in a ceramic<sup>17</sup>. Mathematically, the resonance of  $HEM_{118}$  mode is given as below<sup>18</sup>:

$$f_{r,HEM_{118}} = \frac{6.321c}{\pi D\sqrt{\epsilon_r + 2}} \left[ 0.27 + 0.36 \left( \frac{D}{4H} \right) + 0.02 \left( \frac{D}{4H} \right)^2 \right] \quad (1)$$

The characters “D,” “c,” “ $\epsilon_r$ ” and “H” in the above formula denote the dielectric rod’s diameter, light velocity, permittivity, and height of dielectric, respectively. For the intended ceramic, this formula yields the  $HEM_{118}$  mode resonant frequency at 27.57 GHz. It is nearer to software software-created result.

The axial ratio mutation with different slot shape adjustments is shown in Fig. 4: (a) ring slot coupled ceramic; (b) C-shaped slot coupled ceramic; and (c) C-shaped slot with dual stubs coupled ceramic. It can be observed from Fig. 4 that the C-formed aperture and C-shaped slot, along with dual stubs, reduce the axial ratio below 5 dB and 3dB, respectively. C-shaped slot with dual stubs produces the orthogonal mode with  $90^\circ$  phase shifts within the dielectric, which is an essential condition for circularly polarised waves<sup>5</sup>.

With the parallel positioning, one port is now transformed into a twin port. The S-parameter change with solo and 2-port aerials is shown in Fig. 5. It shows that the  $|S_{11}|$  fluctuation is almost identical for both solo and twin-port aerials. In the operating regime, the mutual coupling level is below  $-25$  dB.

Over the double-port aerial, a metasurface (MS) is now installed. It is created by arranging unit cells periodically. The unit cell’s permeability/permittivity curve between working spectrum is shown in Fig. 6. The following MATLAB program formulation is used to achieve this<sup>19</sup>:

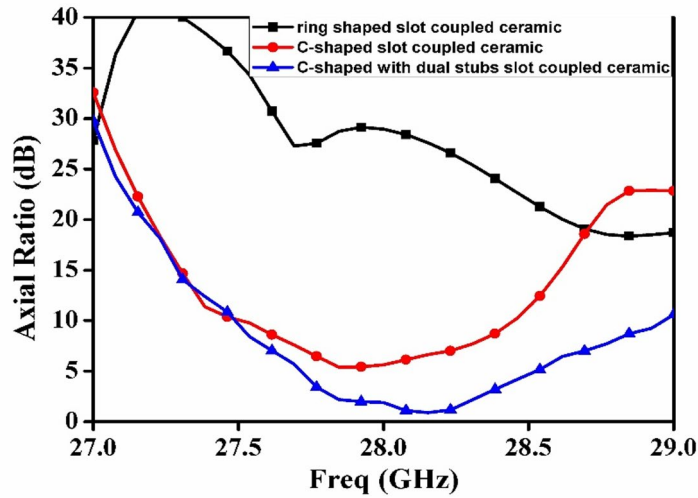


Fig. 4. Axial ratio variation with alteration in the slot’s shape.

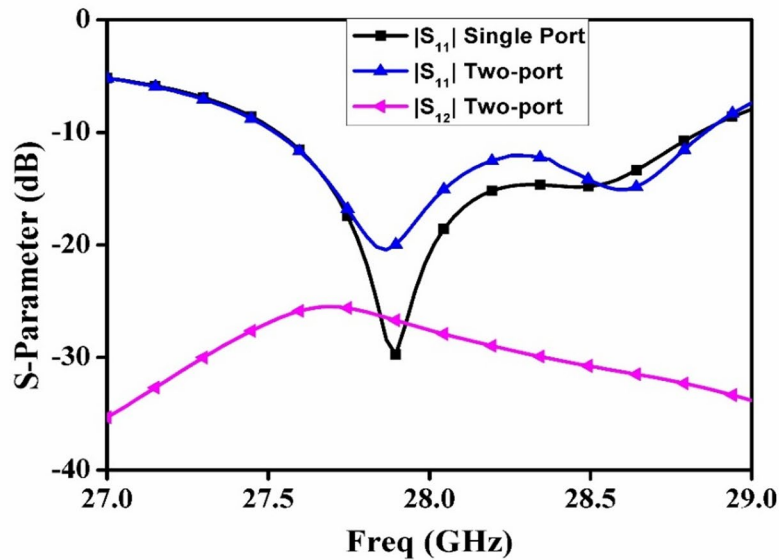


Fig. 5. Variation in S-parameters for one and two-port radiator.

$$Z = \pm \left[ \frac{(1+S_{11})^2 - S_{21}^2}{(1-S_{11})^2 - S_{21}^2} \right]^{0.5} \tag{2}$$

$$e^{j\eta k_0 d} = \frac{S_{21}}{1 - S_{11} \frac{Z-1}{Z+1}} \tag{3}$$

$$\epsilon = \frac{\eta}{Z} \tag{4}$$

$$\mu = Z * \eta \tag{5}$$

“ $\eta$ ,” “ $d$ ,” “ $k_0$ ,” and “ $Z$ ” stand for refractive index, substrate depth, phase constant, and standardized impedance, respectively, in the equations above. As seen in Fig. 6, permittivity and permeability (real/imaginary) are negative throughout the operating span. It suggests that a double negative group is the role of the proposed metasurface.

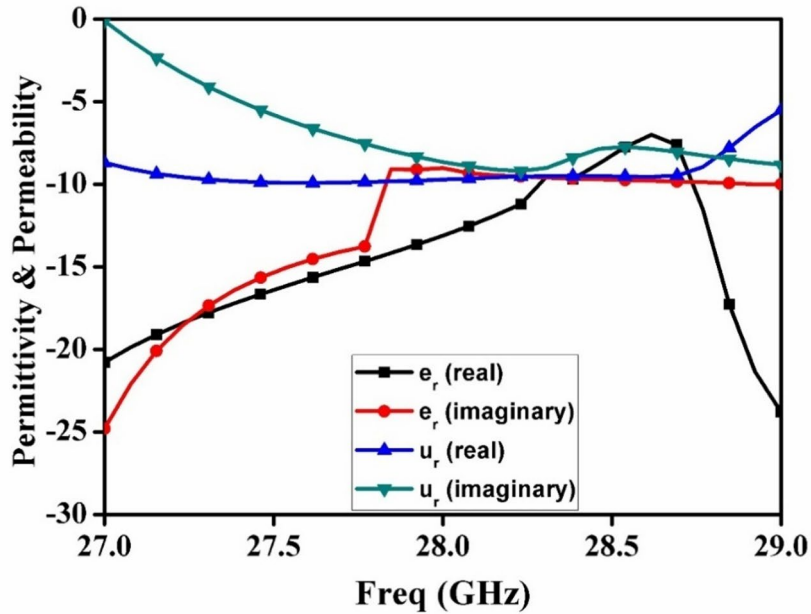


Fig. 6. Permeability/permittivity alteration of the designed unit cell.

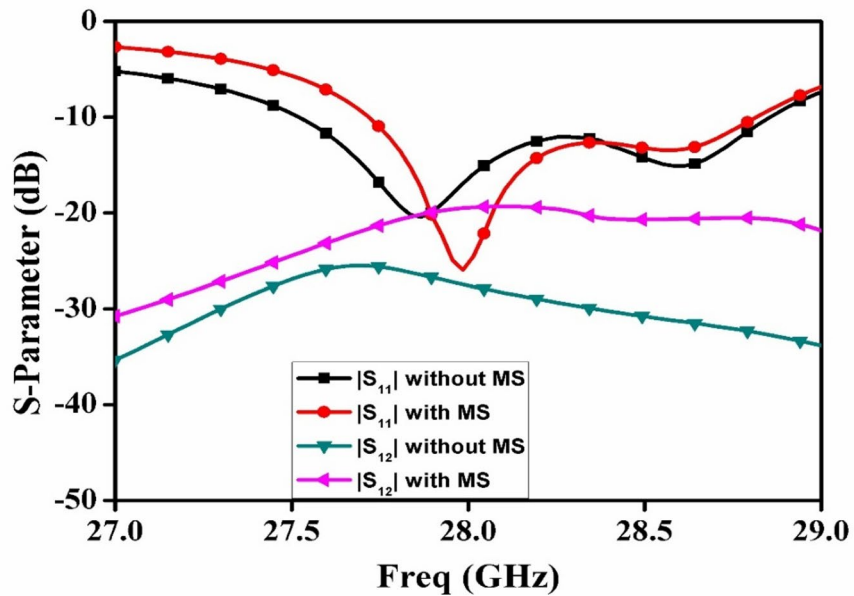


Fig. 7. S-parameter change in occurrence and non-occurrence of metasurface.

The real parts of permittivity ( $\epsilon'$ ) and permeability ( $\mu'$ ) can become negative in materials that exhibit resonant behaviour. The imaginary parts ( $\epsilon''$  and  $\mu''$ ) represent losses. By convention, they are usually positive for passive media, as they correspond to energy dissipation. However, negative imaginary parts can arise in the presence of active or gain media.

Figure 7 shows the S-parameter variation in the occurrence and non-occurrence of the metasurface. It can be detected from Fig. 7 that  $|S_{11}|$  is approximately the same in both instances. There is a slight enhancement in coupling (below -20 dB) after placing the metasurface. This is due to EM coupling between the antenna and the

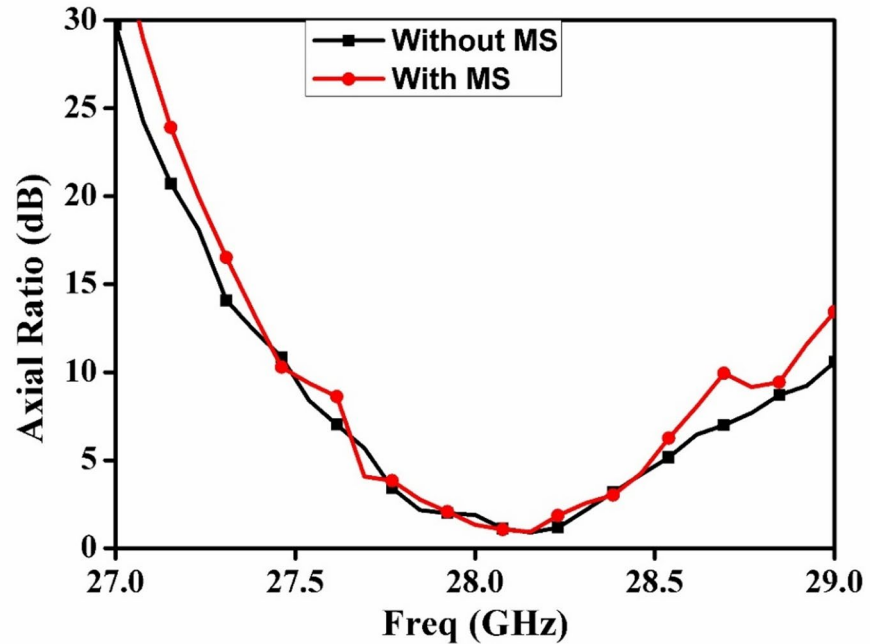


Fig. 8. Axial Ratio alteration occurrence and non-occurrence of metasurface.

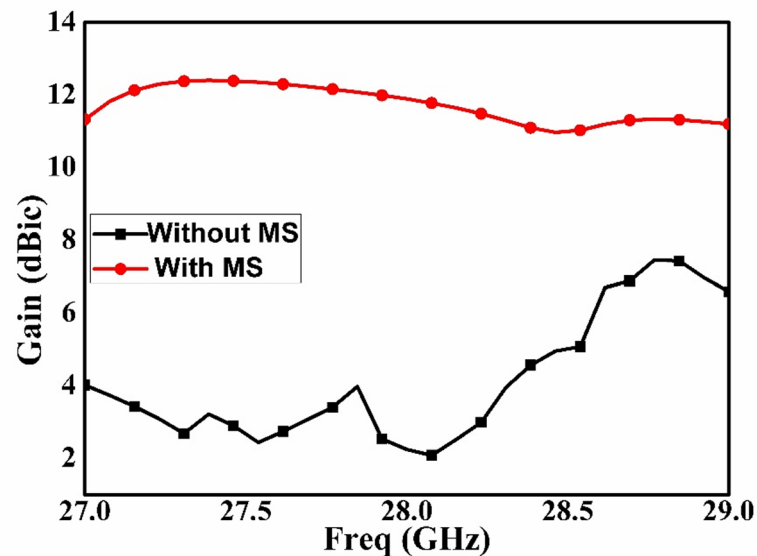
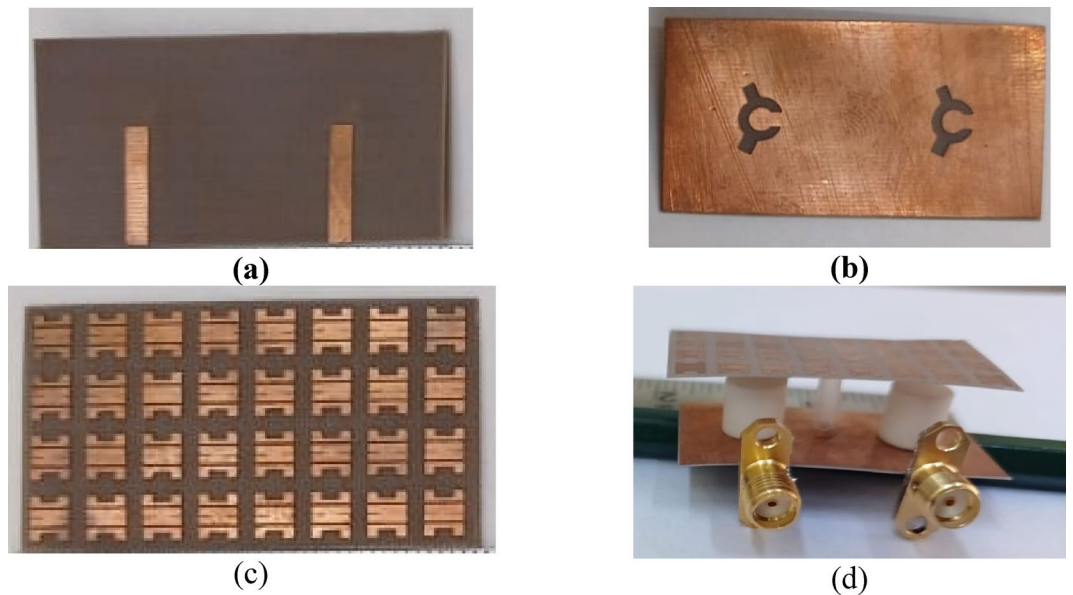


Fig. 9. Change in Gain with occurrence and non-occurrence of metasurface.

metasurface. The axial ratio fluctuation in the broadside position is seen in Fig. 8. It shows that the axial ratio change is nearly the same in both instances.

The gain variation with the occurrence and non-occurrence of the metasurface is seen in Fig. 9. The data given indicate a broader gain enhancement within the operating region. The DNG metasurface raises the gain value to around 11.0 dBic by boosting the aerial's directivity<sup>19</sup>. A double-negative metasurface introduces a negative phase shift, which can compensate for the phase lag of the antenna's radiating fields. This results in



**Fig. 10.** Pictures of Antenna Prototype (a) Microstrip line feed (b) Aperture Coupling (c) Metasurface (d) 3D View.

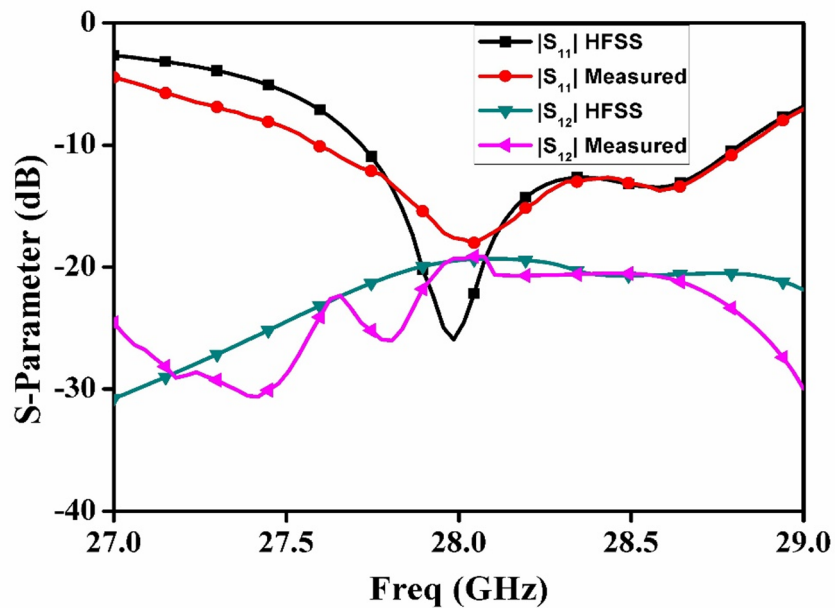


**Fig. 11.** Simulated/Experimental S-parameter alteration for proposed design.

constructive interference in the broadside direction, leading to a narrower main lobe and higher directivity, which translates to increased gain.

### Experimental authentication

This part completely combines diversity factors along with the tested outcomes of the intended 2-port antenna augmented with MS. The produced prototype is revealed in Fig. 10. The RT Duroid base is applied to design the antenna prototype. The computer-generated and tested S-parameters are revealed visually in Fig. 11. The data indicate that the aerial operates efficiently in the 27.65–28.75 GHz range, and the coupling level is consistently below  $-25$  dB over the operating range.

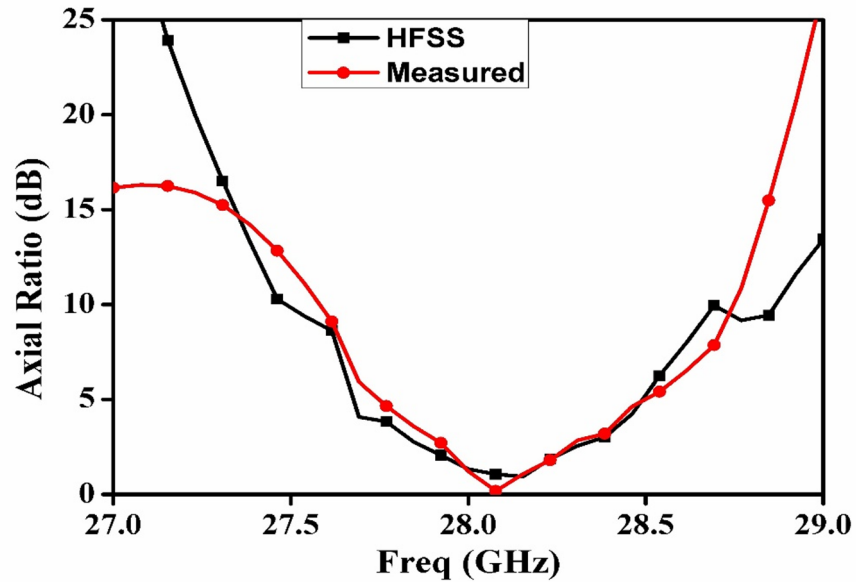


Fig. 12. Measured/Simulated Axial Ratio alteration towards broadsided direction.

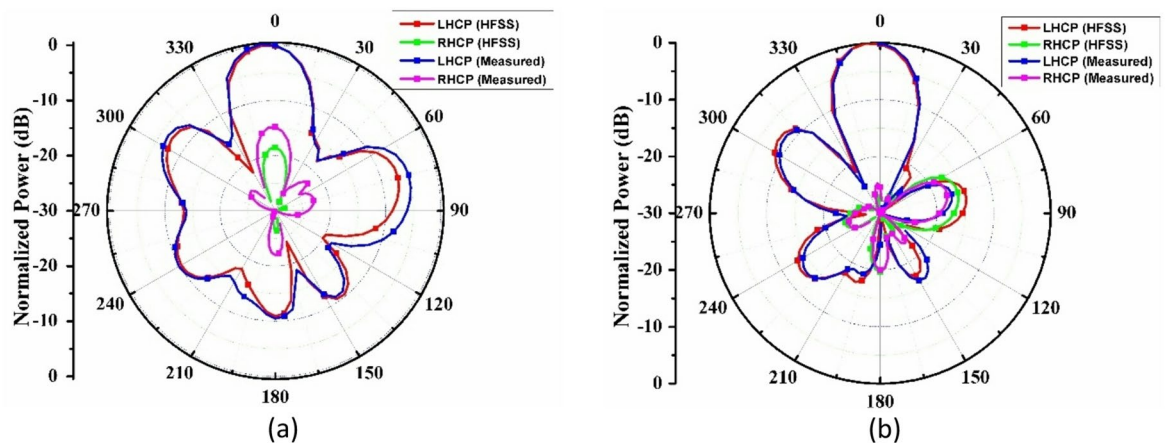


Fig. 13. LHCP/RHCP pattern in XZ plane at 28.0 GHz (a) Port-1 (b) Port-2.

Figure 12 displays simulated and experimental axial ratio modification in a broadsided location. It is calculated in the anechoic chamber using dual linear pattern analysis<sup>5</sup>. The simulated and tested axial ratio patterns show a good correlation, as seen in Fig. 13. The planned aerial supports the working spectrum for CP waves, which is between 27.8 and 28.45 GHz.

The tested and computer-generated LHCP and RHCP fields at 28.0 GHz with port-1/2 in the XZ plane are shown in Fig. 13. Upon observing the pattern, it becomes evident that it is broadsided and directional. Finally, for both ports, LHCP is more powerful than RHCP. This indicates that the aerial is left-handed CP. Figure 14 displays the simulated and tested gain alteration for the proposed antenna. It is measured with the use of two antenna approaches<sup>5</sup>. A decent match between the computer-generated and tested gain change is seen in Fig. 14. The maximum gain that may be achieved within the operational spectrum is roughly 11.0 dBic.

The comparison of the developed mm-wave radiator with the existing mm-wave multi-port radiator built using ceramic is shown in Table 1. The characteristics of gain, impedance/CP bandwidth are considered for comparison. The intended multi-port dielectric radiator outperforms the existing one, as Table 1 demonstrates. Envelop Correlation Coefficient (ECC) and diversification Gain (DG) are the two essential diversification measures. ECC talks about the similar stuffings between the antenna ports. The ECC value of an efficient aerial should be small ( $> 0.1$ ) within the operating range<sup>2</sup>. Similarly, the DG talks about the MIMO gain in a fading situation. The DG value should be around 10 dB within the operating region<sup>2</sup>. Figure 15 shows the ECC and DG

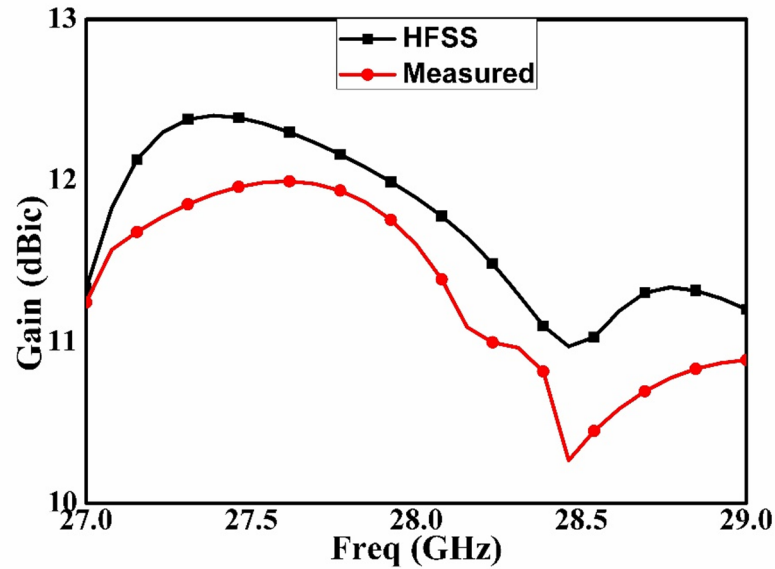


Fig. 14. Simulated/Experimental gain modification of planned antenna.

Aerial layout	No. of ports	Operating bandwidth (GHz)	AR bandwidth (GHz)	Gain (dBi/dBic)
Rectangular dielectric <sup>6</sup>	02	1.34	NA	8.0
Rectangular dielectric <sup>7</sup>	02	2.4	NA	6.0
Rectangular dielectric <sup>8</sup>	04	2.23	NA	7.0
Cylindrical dielectric <sup>9</sup>	02	4.2	NA	4.0
Rectangular dielectric <sup>10</sup>	02	3.15	NA	8.0
Cylindrical dielectric <sup>11</sup>	02	2.29	0.33	5.0
Cylindrical dielectric <sup>12</sup>	02	0.6	NA	4.5
<b>Planned Aerial</b>	<b>02</b>	<b>1.10</b>	<b>0.65</b>	<b>11.0</b>

Table 1. Comparison of the planned radiator with the existing millimeter-wave antenna constructed using  $\text{Al}_2\text{O}_3$  Dielectric.

change for the desired antenna as measured and projected. These parameters are measured using S-parameters<sup>2</sup>. It demonstrates that the ECC and DG are below 0.02 and about 10 dBi, respectively, over the operational range.

## Conclusion

A 2-port ceramic aerial, along with a metasurface lens, has been designed and investigated. With the help of aperture coupling,  $\text{HEM}_{116}$  mode is stimulated inside the ceramic. It allows the aerial to work within 27.65–28.75 GHz. Feed design also creates a CP feature within the working regime i.e., 27.8–28.45 GHz. A metasurface, having negative permittivity and permeability, is appended over a 2-port aerial to advance the gain value by 12 dBi. Broad-sided radiation features, as well as a good value of ECC/DG, make the planned radiator suitable for licensed 5G FR2 wireless systems.

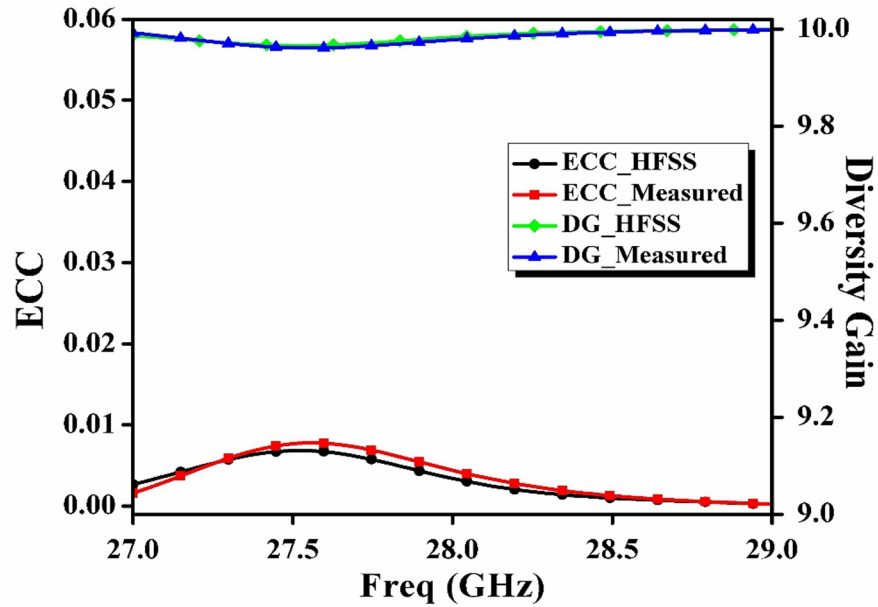


Fig. 15. Experimental/Simulated ECC and DG variation.

### Data availability

The datasets used and/or analysed during the current study are available from the corresponding author upon reasonable request.

Received: 22 September 2025; Accepted: 3 November 2025

Published online: 08 December 2025

### References

- Hong, W. Solving the 5G mobile antenna puzzle: assessing future directions for the 5G mobile antenna paradigm shift. *IEEE Microw. Mag.* **18** (7), 86–102 (2017).
- Sharawi, M. S. Printed MIMO Antenna Engineering Artech House (Boston, London, 2014).
- Kornprobst, J., Wang, K., Hamberger, G. & Eibert, T. F. A mm-Wave patch antenna with broad bandwidth and a wide angular range. *IEEE Trans. Antennas Propag.* **65**(8), 4293–4298 (2017).
- Petosa, A. *Dielectric Resonator Antenna Handbook* (Artech House, 2007).
- Balanis, C. A. *Antenna Theory: Analysis and Design* (Wiley, 2016).
- Zhang, Y., Deng, J. Y., Li, M. J., Sun, D. & Li-Xin Guo A MIMO dielectric resonator antenna with improved isolation for 5G mm-Wave applications. *IEEE Antennas. Wirel. Propag. Lett.* **18**, 747–751 (2019).
- Pan, Y. M. & Qin, X. Sun and Shao Yong Zheng A simple decoupling method for 5G Millimeter-Wave MIMO dielectric resonator antennas. *IEEE Trans. Antennas Propag.* **67** (4), 2224–2234 (2019).
- Nimmagadda, S. & Murthy Improved isolation metamaterial inspired mm-Wave MIMO dielectric resonator antenna for 5G application. *Progress Electromagnet. Res. C.* **100**, 247–261 (2020).
- Hasan, M. L., Mabrouk, I. B., Almajali, E. R. F., Nedil, M. & Denidni, T. A. Hybrid isolator for Mutual-Coupling reduction in Millimeter-Wave MIMO antenna systems. *IEEE Access.* **7**, 58466–58474 (2019).
- Alanazi, M. D. & Khamas, S. K. A compact dual band MIMO dielectric resonator antenna with improved performance for mm-Wave applications. *Sensors* **22**, 5056 (2022).
- Kumar, A., Dwivedi, A. K. & Nagesh, K. N. Anand Sharma and Pinku Ranjan circularly polarized dielectric resonator based two Port Filtenna for Millimeter-Wave 5G communication system. *IETE Tech. Rev.* **39**, 1501–1511 (2022).
- Darshika Sharma, R. et al. Dielectric resonator-based two-port Filtennas with pattern and space diversity for 5G IoT applications. *Int. J. Microw. Wirel. Technol.* **15**, 263–270 (2022).
- Dewangan, L. & Mishra, N. K. Isolation enhancement of MIMO dielectric antenna using  $\epsilon$ -Negative metamaterial dielectric superstrate for NR-78 band. *IEEE Trans. Dielectr. Electr. Insul.* **32**, 1987–1996 (2025).
- Mishra, N. K., Acharjee, J., Sharma, V., Tamrakar, C. & Dewangan, L. Mutual coupling reduction between the cylindrical dielectric resonator antenna using split ring resonator-based structure. *AEU - Int. J. Electron. Commun.* **154**, 154305 (2022).
- Ibrahim, A. A. et al. Compact Four-Port Circularly Polarized MIMO X- DRA *Sens.* **22**(12), 4461 (2022).
- Mahmoud, A., Ahmed, M. I., Varshney, G. & Ibrahim, A. A. An array of staircase-shaped circularly polarized DRA. *Int. J. RF Comput. Aided Eng.* **31**, 1–9 (2021).
- Kajfez, D., Glisson, A. W. & James, J. Computed modal field distributions for isolated dielectric resonators. *IEEE Trans. Microw. Theory Tech.* **32**, 1609–1616 (1989).
- Mongia, R. K. Dielectric resonator antennas—A review and general design relations for resonant frequency and bandwidth. *Int. J. Microw. Millimeter-Wave Computer-Aided Eng.* **4** (3), 230–247 (1994).
- Numan, A. B. Sharawi, Extraction of material parameters for metamaterials using a full-wave simulator [education column]. *IEEE Antennas Propag. Mag.* **55** (5), 202–211 (2013).

### Author contributions

Conceptualization and Methodology [Sateesh Kumar Yadav and Ajay Kumar Dwivedi]; Writing - revised draft preparation: [Shivesh Tripathi, Anand Sharma]; Analysis and Investigation: [Ajay Kumar Dwivedi and Deepak Sigroha]; Writing - original draft preparation and Supervision: [Stuti Pandey].

### Funding

Open access funding provided by Manipal University Jaipur.

### Declarations

### Competing interests

The authors declare no competing interests.

### Consent for publication

I, Stuti Pandey, give my consent for the publication of identifiable details, which can include photograph(s) and/or videos and/or figures and/or details within the text (“Material”) to be published in the above Journal and Article.

### Additional information

**Correspondence** and requests for materials should be addressed to S.P.

**Reprints and permissions information** is available at [www.nature.com/reprints](http://www.nature.com/reprints).

**Publisher’s note** Springer Nature remains neutral with regard to jurisdictional claims in published maps and institutional affiliations.

**Open Access** This article is licensed under a Creative Commons Attribution-NonCommercial-NoDerivatives 4.0 International License, which permits any non-commercial use, sharing, distribution and reproduction in any medium or format, as long as you give appropriate credit to the original author(s) and the source, provide a link to the Creative Commons licence, and indicate if you modified the licensed material. You do not have permission under this licence to share adapted material derived from this article or parts of it. The images or other third party material in this article are included in the article’s Creative Commons licence, unless indicated otherwise in a credit line to the material. If material is not included in the article’s Creative Commons licence and your intended use is not permitted by statutory regulation or exceeds the permitted use, you will need to obtain permission directly from the copyright holder. To view a copy of this licence, visit <http://creativecommons.org/licenses/by-nc-nd/4.0/>.

© The Author(s) 2025